

We are IntechOpen, the world's leading publisher of Open Access books Built by scientists, for scientists

5,800

Open access books available

142,000

International authors and editors

180M

Downloads

Our authors are among the

154

Countries delivered to

TOP 1%

most cited scientists

12.2%

Contributors from top 500 universities



WEB OF SCIENCE™

Selection of our books indexed in the Book Citation Index
in Web of Science™ Core Collection (BKCI)

Interested in publishing with us?
Contact book.department@intechopen.com

Numbers displayed above are based on latest data collected.
For more information visit www.intechopen.com



Chapter

Micro-Thermoelectric Generators: Material Synthesis, Device Fabrication, and Application Demonstration

*Nguyen Van Toan, Truong Thi Kim Tuoi, Nguyen Huu Trung,
Khairul Fadzli Samat, Nguyen Van Hieu and Takahito Ono*

Abstract

Micro-thermoelectric generator (TEG) possesses a great potential for powering wireless Internet of Things (IoT) sensing systems due to its capability of harvesting thermal energy into usable electricity. Herein, this work reviews the progress in recent studies on the micro-TEG, including material synthesis, device fabrication, and application demonstration. Thermoelectric materials are synthesized by the electrochemical deposition method. Three kinds of high-performance thermoelectric materials, including thick bulk-like thermoelectric material, Pt nanoparticles embedded in a thermoelectric material, and Ni-doped thermoelectric material, are presented. Besides the material synthesis, novel fabrication methods for micro-TEG can also help increase its output power and power density significantly. Two fabrication processes, micro/nano fabrication technology and assembly technology, are investigated to produce high-performance micro-TEG. Moreover, the fabricated micro-TEG as a power source for portable and wearable electronic devices has been demonstrated successfully.

Keywords: thermal-to-electric energy conversion, micro-thermoelectric generator, thermoelectric materials, micro/nano fabrication technology, assembly technology

1. Introduction

The considerable growth of research studies in energy-harvesting technologies, such as solar energy harvesting [1], RF power harvesting [2], thermoelectric-generator-based electrolyte [3], thermoelectric-generator-based solid thermoelectric materials [4], associated with the Internet of Things (IoT) leads to more demands in the development of the high performance of a micro-thermoelectric generator (TEG). Micro-TEG keeps a role as a charger to the rechargeable battery of IoT sensing systems or even replaces the battery if micro-TEG with high performance is employed. The TEG utilizes the Seebeck effect that can convert thermal energy into electricity. The

TEG has many advantages, including small size, without moving parts, free from noise, greenhouse gases, and long-term operation time [5, 6]. A voltage will be generated once a temperature difference across the micro-TEG is provided.

To enhance the performance of the micro-TEG, high-performance thermoelectric materials and increasing the number of thermoelectric elements are vital factors. Regarding thermoelectric materials, until now, several thermoelectric materials have been studied, including organic materials (metalloporphyrin/single-walled carbon nanotube composite films [7], Poly(3,4-ethylenedioxythiophene) polystyrene sulfonate [8], and compositions of conducting polymers and metal nanoparticles [9]) and inorganic materials (nanoporous silicon [10], cobalt triantimonide [11], bismuth telluride and antimony telluride [12], tin selenide [13], electrodeposited bismuth telluride [14]). Among them, thermoelectric-materials-based BiTe are widely investigated because of their high performance for applications at near room temperature. For synthesis of thermoelectric-materials-based BiTe, several methods have been reported, including thermally evaporated method [15], metal organic chemical vapor deposition method [16], and pulsed laser melting method [17]. Electrochemical deposition is one of the preferred ways to enable the deposited film with high-quality morphology and compactness. Moreover, the electrodeposition method is capable of modifying the morphology, composition, and crystal structure of the synthesized film, which would result in the high performance of the deposited materials. Concerning enhancing the integration density, hundreds of thermoelectric elements could be produced on a small footprint by utilizing micro/nano fabrication technologies; however, some issues still remain. For instance, a complex process is required to create the air bridge between two thermoelectric elements. High contact resistance between thermoelectric elements and substrate results in low-performance micro-TEG. The performance of thermoelectric materials is degraded during their fabrication of the micro-TEG. The height of the thermoelectric element is limited by micro/nano fabrication technology. Thus, it makes micro-TEG low performance and against the practical applications.

In this work, we review the recent progress in the micro-TEG, including material synthesis, device fabrication, and application demonstration. Various high-performance thermoelectric materials synthesized by the electrodeposition method, including thick bulk-like thermoelectric material, Pt nanoparticles embedded in a thermoelectric material, and Ni-doped thermoelectric material, are presented. In addition, the fabrication of micro-TEGs based on micro/nano fabrication technology as well as assembly technology is demonstrated. The performance of the fabricated micro-TEG is compared with other related works. Moreover, the fabricated micro-TEG as a power source for a calculator and a twist watch has been investigated.

2. Basic principles of thermoelectric generator

2.1 Properties of thermoelectric material

2.1.1 Seebeck coefficient

The Seebeck coefficient is defined as the harvested voltage from the temperature difference across the thermoelectric materials. Its standard unit is microvolts per kelvin ($\mu\text{V/K}$). The Seebeck coefficient may exhibit positive or negative signs, which represents p-type or n-type thermoelectric materials, respectively. The p-type

thermoelectric material shows an excess of holes, while the n-type thermoelectric material possesses an excess of free electrons. When a temperature difference appears at the ends of the thermoelectric material block, the charge carriers (electrons or holes) move from the hot side to the cold side, causing a thermoelectric voltage. The following equation depicts the Seebeck coefficient S of thermoelectric materials:

$$S = \frac{\Delta V}{\Delta T}, \quad (1)$$

where ΔV is the voltage gradient between the hot and cold sides of the thermoelectric material, and ΔT is the temperature difference between two sides.

One factor affecting the Seebeck coefficient is charge carrier concentration n . The relationship between the charge carrier and the Seebeck coefficient is proven experimentally and theoretically by published works [18–20].

$$S = \frac{8\pi^2 k_B^2 T}{3eh^2} m^* \left(\frac{\pi}{3n} \right)^2, \quad (2)$$

where k_B is Boltzmann constant, T is temperature, e is the electron charge, h is Planck constant, and m^* is effective mass.

2.1.2 Electrical conductivity

Electrical conductivity is an essential electrical property for thermoelectric material to conduct an electrical current. Electrical conductivity and electrical resistivity are the reciprocals of each other. Macroscopically, electrical conductivity is related to the dimensions and resistance of the measured thermoelectric material, which can be calculated by the following equation:

$$\sigma = \frac{L}{RA}, \quad (3)$$

where L is the length of the material, R is the resistance of the material, A is the contact area perpendicular to the current direction.

In principle, the electrical resistivity of a material characterizes the ability of the material to interrupt electricity flow. Therefore, it is strongly related to the flow of electrons and holes in a material. Those two factors influence the value of electrical conductivity, as shown in the following equation,

$$\sigma = e (\mu_e n + \mu_h p), \quad (4)$$

where μ_e , n , μ_h , and p symbolize electron mobility, the carrier density of electron, hole mobility, and carrier density of hole, respectively.

2.1.3 Thermal conductivity

The thermal conductivity k of thermoelectric material is dependent on the charge carriers and the phonon's movement. Generally, the total thermal conductivity of metal increases when the electrical conductivity is high due to the directly proportional relation of electrical conductivity with carrier-charge thermal conductivity.

Therefore, the only option to reduce the thermal conductivity is by scrutinizing the value of lattice thermal conductivity [21, 22]. A lower lattice thermal conductivity results in a smaller value of total thermal conductivity. Introducing the nanoparticles in the metal might reduce the lattice thermal conductivity by blocking the excitation stream of lattice vibration, also known as phonons flow. The interrupted phonons flow increases the phonon scattering and elongates the phonon wavelength. Therefore, the time taken for the heat to transfer will be increased. The total thermal conductivity can be expressed by considering those two factors (charge carriers and lattice), as the following equation,

$$k = k_l + k_e, \quad (5)$$

where k_l and k_e are lattice and charge carrier thermal conductivity, respectively. Equation of lattice thermal conductivity can be referred to the following relationship.

$$k_l = DC_p\rho, \quad (6)$$

where D , C_p , and ρ signify thermal diffusivity, specific heat, and material density, respectively.

Equation of charge-carriers thermal conductivity is estimated by

$$k_e = ne\mu L_f T, \quad (7)$$

where n is carrier concentration, e is the electron charge, μ is carrier mobility, L_f is Lorenz factor ($2.44 \times 10^{-8} \text{ W}\Omega\text{K}^{-2}$), and T is temperature.

2.1.4 Figure of merit

The figure of merit ZT is an instrument to evaluate the performance of thermoelectric materials, which encompassed the factor of the Seebeck coefficient S , electrical conductivity σ , thermal conductivity k , and absolute temperature T of the thermoelectric material. The ZT is defined as follows:

$$ZT = \frac{\sigma S^2 T}{k} \quad (8)$$

To obtain high ZT values of thermoelectric materials, high S and large σ are desired; however, there is a trade-off between S and σ , as shown in Eqs. (2) and (4). Therefore, adjusting the coefficient between S and σ is a critical technique to achieve the highest ZT . Lowering thermal conductivity is also an important point to enhance the ZT , which can avoid the thermal shortcut problem and maintain a large temperature difference between the two sides.

2.2 Thermoelectric generator structure

A TEG is a solid device, which is able to convert thermal energy into electricity or vice versa. It consists of n and p-type thermoelectric elements arranged electrically in series and thermally in parallel. A cross-sectional view and titled view of the TEG structure are shown in **Figure 1(a)** and **(b)**, respectively. It mainly consists of n- and p-type thermoelectric elements, a metal bar, and a substrate.

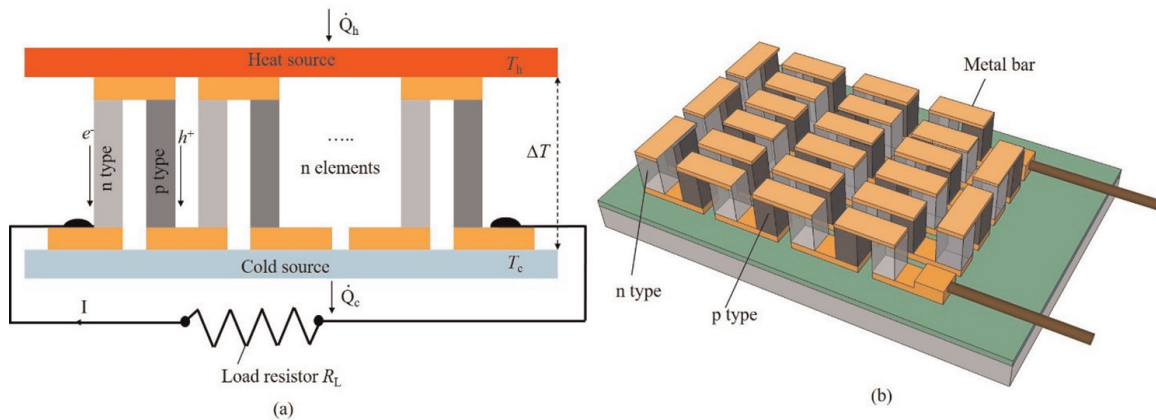


Figure 1. TEG structure. (a) Cross-sectional view. (b) Titled view.

As mentioned previously, the p-type element has a positive Seebeck coefficient and an excess of holes h^+ . The n-type element has a negative Seebeck coefficient and an excess of free electrons e^- . The two elements are connected by an electrical conductor forming a junction, usually a copper strip. When a load resistor R_L is connected in the output terminal of the micro-TEG, an electrical circuit is created. A potential voltage across the resistor is generated once the electrical current flows. The micro-TEG will create the current when a temperature difference across the micro-TEG appears. Higher temperature difference ΔT results in the larger electric output power.

The resistance of the thermoelectric elements is estimated by:

$$R = n \left(\rho_n \frac{L_n}{A_n} + \rho_p \frac{L_p}{A_p} \right) \quad (9)$$

where ρ_n and ρ_p are the electrical resistivity of n and p-type thermoelectric material, respectively, L_n and L_p are the height of n- and p-type thermoelectric elements, respectively, and A_n and A_p are the cross-sectional area of n and p-type thermoelectric elements, respectively.

In the above Eq. (10), the electrical contact resistance is eliminated. However, this resistance is typically quite difficult to be negligible due to the fabrication process. Therefore, the electrical contact resistance R_a should be counted.

$$R = n \left(\rho_n \frac{L_n}{A_n} + \rho_p \frac{L_p}{A_p} \right) + R_a \quad (10)$$

The generated voltage V_{TEG} could be estimated by the following equation:

$$V_{TEG} = n(S_p - S_n) \Delta T \quad (11)$$

where n is the number of thermoelectric elements, S_p and S_n are the Seebeck coefficient of p and n types thermoelectric materials, respectively, and ΔT is a temperature difference across the thermoelectric elements.

The maximum electrical output power of the TEG can be calculated by using Eq. (13), which is obtained if a load resistance R_L is equal to the equivalent internal resistance of thermoelectric elements in series [23].

$$P_{max} = n \frac{(S_p - S_n)^2 \Delta T^2}{4R_L} = \frac{nA}{h} \frac{(S_p - S_n)^2 \Delta T^2}{4(\rho_p + \rho_n)} \quad (12)$$

where A and h are a cross-sectional surface area and height of thermoelectric elements, respectively. ρ_p and ρ_n are the electrical resistivities of p-type and n-type thermoelectric materials.

Several factors could affect the performance of the TEGs. Thermoelectric materials with excellent characteristics, including a high Seebeck coefficient, a small electrical resistivity, and a low thermal conductivity, are always desired for enhancing the TEG's performance. Many novel approaches, including utilizing metal nanoparticles [24], nanoporous materials [25], carbon black particles [26], and metal doping [27, 28], have been investigated to improve thermoelectric material's properties. Besides the effects of material properties, selecting proper physical dimensions of thermoelectric elements, such as the width and height of thermoelectric elements, could also contribute to better performance of the TEG [28]. Also, increasing the number of thermoelectric elements would be a valuable method for improving the performance of the TEG, as shown in Eq. (13).

The formula of an electrical energy conversion efficiency η_{TEG} of the TEG [29] is defined by Eq. (14), which indicates that high electrical efficiency of the TEG could be achieved by a high figure of merit ZT as well as a large temperature difference ΔT .

$$\eta_{TEG} = \frac{\Delta T}{T_H} \frac{\sqrt{1 + ZT} - 1}{\sqrt{1 + ZT} + \frac{T_C}{T_H}}, \quad (13)$$

where T_H and T_C are the hot and cold temperatures of TEG, respectively.

3. Material synthesis

3.1 Electrodeposition method

Thermoelectric materials presented in this work are synthesized by the conventional three-electrode system, which is controlled electrochemically by a potentiostat. The system involves a working electrode, a counter electrode, and a reference electrode. A silicon wafer with Cr-Au layers on the top insulated by SiO_2 layer is employed as a working electrode, while a Pt strip and Ag/AgCl with 3 M KCl solution are utilized as counter and reference electrodes. The synthesized material is formed on the working electrode caused by the oxidation–reduction (redox) reaction. The electrochemical deposition mechanism is quite complicated and has been presented in many publications [30, 31]. It can be summarized as follows. In the electrolyte, the absorbed atom is in the form of the hydrated matter, which is stripped at the interface between the solution and the cathode. Then, it combines with other absorbed atoms to form a new nucleus. This process continues and contributes to the further growth of the deposited material.

One of the benefits of the electrodeposition method is the ability to change the morphology, composition, and crystal structure of deposited film by adjusting certain parameters in the electrodeposition system. All the changes might influence the alteration of the electronic or/and thermal properties of the deposited film. The effectively applied potential on the working electrode is one of the important parameters in the

electrodeposition system that reflect on the variation of the current density. A change of the over potential on the electrode normally affects the current density and a chance to change the morphology.

3.2 Thick bulk-like thermoelectric material

As mentioned in the introduction section, thermoelectric materials could be synthesized by several methods. Although high performance of thin-film thermoelectric materials has been achieved, the TEG produced by thin-film thermoelectric materials possesses a low output power. Once the height of thermoelectric elements is low (a few micrometer heights), it is hard to create a large temperature difference across the TEG device. Thus, its output voltage, as well as output power, is in small value. The evidence could be easily seen via Eqs. (12) and (13). Although an output power of the TEG-utilized thin films could be enhanced by a novel design for heat transfer in a lateral direction, TEG's output power is still not enough for realistic applications. Therefore, a thick film of thermoelectric material with high Seebeck, large electrical conductivity, and low thermal conductivity are always desired to achieve high-performance micro-thermoelectric generators. Typically, thick thermoelectric material films could be formed by a screen printing method, a powder synthesis and sintering method, and a mechanical alloying and spark plasma sintering method; nevertheless, these methods have at least the following disadvantages, such as poor mechanical strength, a high fabrication cost, and low material performance. Herein, we present the thick and stable thermoelectric films synthesized by electrodeposition.

Figure 2 shows the sample preparation process for material synthesis and material evaluation. It starts from a silicon substrate with a thickness of 300 μm (**Figure 2(a)**).

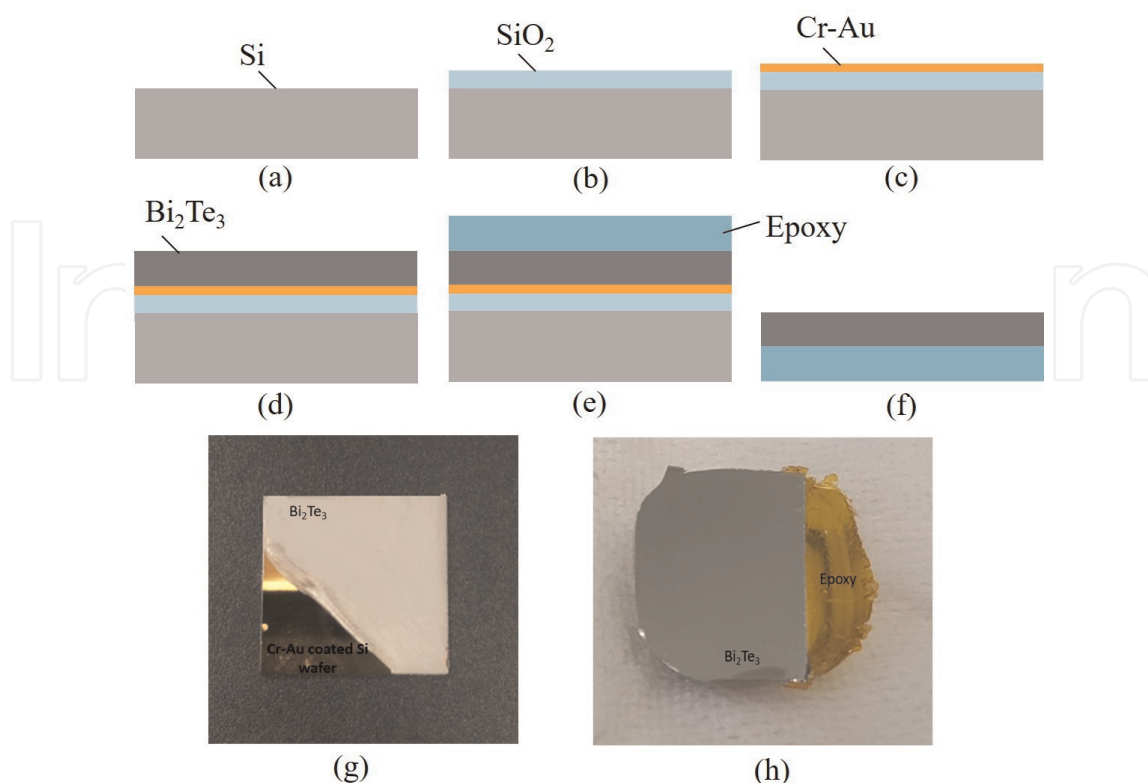


Figure 2. Sample preparation process. (a) Silicon. (b) SiO₂ deposition. (c) Cr-Au deposition. (d) Thermoelectric material formed by electrodeposition. (e) Epoxy coating. (f) Sample for evaluation.

On top of this substrate, a SiO_2 layer with a thickness of 200 nm is deposited by a plasma-enhanced chemical vapor deposition (PECVD) employing TEOS (TetraEthOxySilan Si $(\text{OC}_2\text{H}_5)_4$), as shown in **Figure 2(b)**. Next, Cr-Au layers with a thickness of 20 nm and 150 nm are formed on the SiO_2 layer by the sputtering method, respectively (**Figure 2(c)**). The thermoelectric material is subsequently deposited by the electrodeposition method, as discussed in Section 3.1 (**Figure 2(d)**). Because a material property evaluation needs to be conducted on an insulating substrate to avoid short-circuiting, the synthesized films are peeled off from the substrate by epoxy resin, as shown in **Figure 2(e)** and **(f)**. **Figure 2(g)** and **(h)** show the electrodeposited thermoelectric material (Bi_2Te_3) on the silicon substrate and transferred thermoelectric material on epoxy, respectively.

Figure 3(a) and **(b)** show the electrodeposited thermoelectric materials by constant and pulsed conditions, respectively. As can be seen that, the constant electrodeposited film (**Figure 3(a)**) exhibits an initial 4 μm -thick compact layer while the top layer includes pillar structures. Although the thick-film thermoelectric material can be achieved by further deposition, its mechanical strength is very weak due to its porous structure. The thick electrodeposited film by the constant condition is easily peeled off for substrate. To overcome this problem, pulsed electrodeposition has been conducted. Compared with the constant electrochemical deposition, the pulsed electrodeposition with a pulse delay time for the recovery of the ion concentration always leads to a crystalline structure with high orientation and good uniformity [32]. This is proven in **Figure 3(b)**. The deposited surface under pulsed conditions is more uniform and smoother than that under constant conditions. **Figure 3(c)** shows a representative cross-sectional SEM image of the 600 μm -thick Bi_2Te_3 electrodeposited film, which is comparable to the bulk Bi_2Te_3 material. Consequently, by using simple and

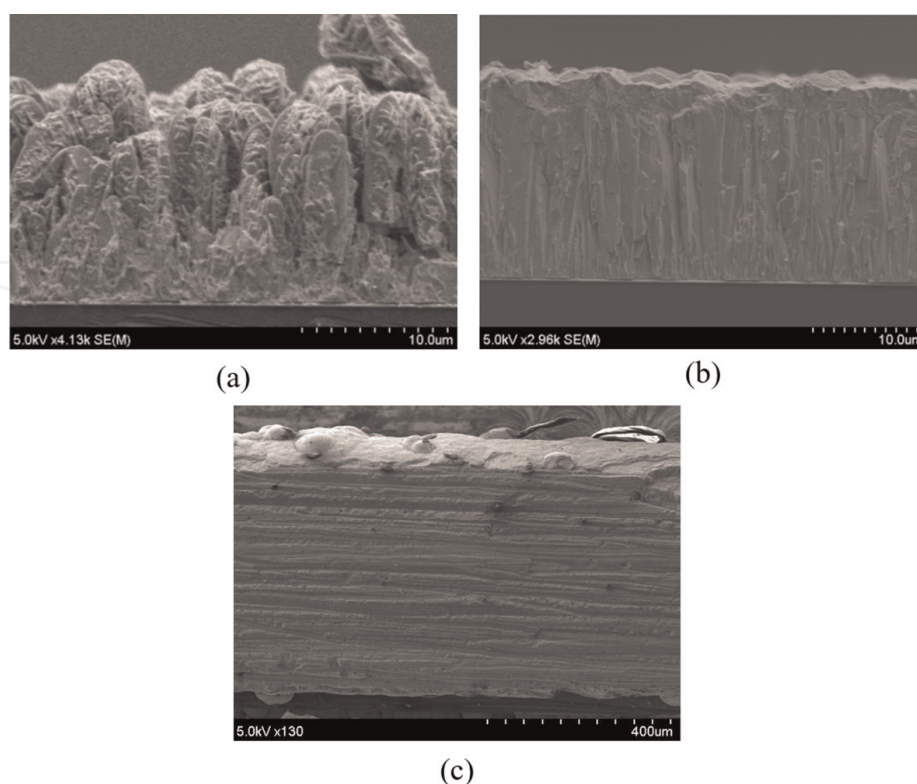


Figure 3. Thermoelectric material. (a) Constant deposition. (b) Pulsed deposition. (c) A 600 μm -thick Bi_2Te_3 electrodeposited film.

	Constant electrodeposition		Pulsed electrodeposition	
	Nonannealing	Annealing (250°C)	Nonannealing	Annealing (250°C)
Seebeck coefficient ($\pm 20 \mu\text{V/K}$)	-50	-110	-80	-150
Electrical resistivity ($\pm 5 \mu\Omega\text{m}$)	50	20	20	15
Power factor (W/mK^2)	0.5×10^{-4}	6×10^{-4}	3.2×10^{-4}	15×10^{-4}

Table 1.
Electrodeposited thermoelectric material properties.

low-cost electrochemical deposition technique, thick bulk-like thermoelectric material posing a highly compact and uniform appearance could be achieved.

Thermoelectric material properties, including Seebeck coefficient and electrical resistivity, are evaluated, as shown in **Table 1**. The pulsed deposited film has a higher Seebeck coefficient as well as lower electrical resistivity than those of the constant deposited film. The power factor for pulsed deposited material is $3.2 \times 10^{-4} \text{ W/mK}^2$ while it is $0.5 \times 10^{-4} \text{ W/mK}^2$ for constant deposited material. Moreover, an annealing process has been performed to enhance the characteristics of the electrodeposited thermoelectric materials. The highest Seebeck coefficient is found at the annealing temperature of 250°C. The details of measurement setup and evaluation results can be found in [33].

In summary, thick bulk-like thermoelectric material based on the electrochemical deposition technique has been demonstrated. The electrodeposited film possesses a highly compact and uniform surface. The electrodeposited material properties by pulsed deposition are much higher than those by constant deposition. Also, thermoelectric performances of the electrodeposited film enhanced by the annealing process have been investigated.

3.3 Platinum nanoparticles embedded in thermoelectric material

Metal nanoparticle inclusion in the nanocomposite process is one of the promising methods to enhance the figure of merit ZT . However, there are a limited number of research studies on metal nanoparticle inclusion to improve thermoelectric material in film condition, especially through the synthesis of the electrochemical deposition. Au nanoparticle- Bi_2Te_3 nanocomposite has been demonstrated in [34], which is synthesized by a chemical-solution-based bottom-up method at low temperature. The ZT reaches up to 0.95 at 450 K [34]. A similar technique has been applied successfully for the Ag nanoparticle- Bi_2Te_3 nanocomposite, as shown in [35]. Nevertheless, its performance only improved significantly at a high-temperature region while at room temperature, its performance is just a half that of the pure Bi_2Te_3 because of the lower value of the Seebeck coefficient resulting in a smaller the ZT value. Herein, we select the Pt nanoparticles for embedding to Bi_2Te_3 because it has been proven by [36]. In this reference, the Pt nanoparticles have been embedded in Sb_2Te_3 , which can enhance the Seebeck coefficient by filtering the low-energy carriers caused by band-bending potential formation, thus improving the power factor. Moreover, the Pt nanoparticles can help reduce the thermal conductivity due to scattering the mid- to long-wavelength phonons. Therefore, the ZT of nanocomposite thermoelectric material is much higher than that of pure thermoelectric material.

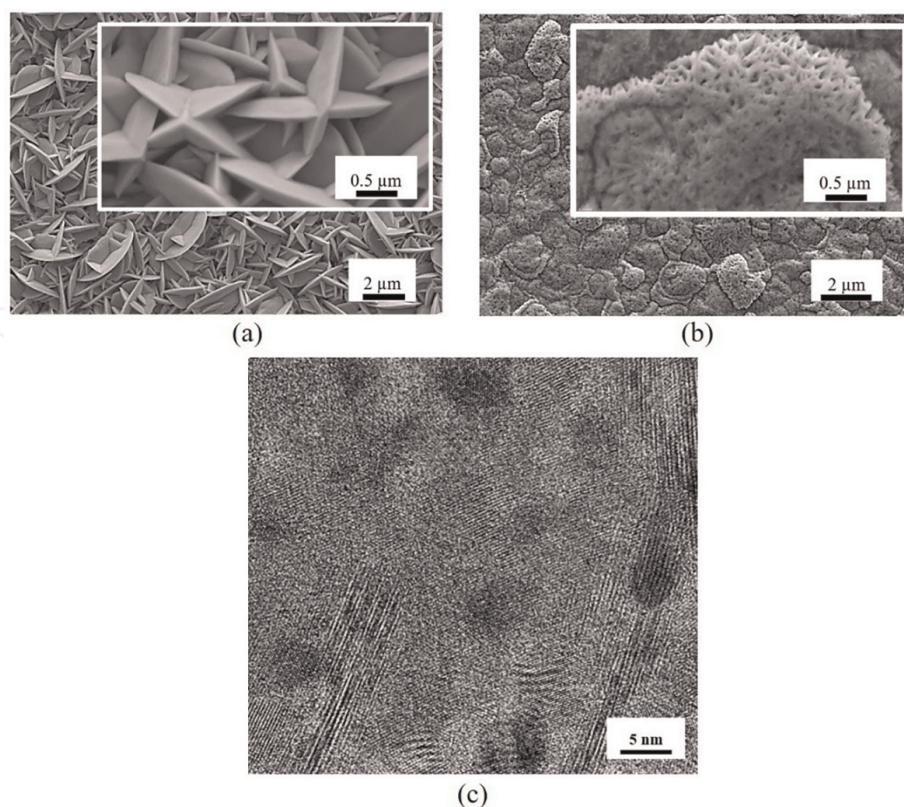


Figure 4. (a) Electrodeposited surface of Bi_2Te_3 . (b) Electrodeposited surface of $\text{Pt-Bi}_2\text{Te}_3$. (c) High resolution of TEM image of $\text{Pt-Bi}_2\text{Te}_3$.

Figure 4(a) shows the surface morphology of the electrodeposited pure Bi_2Te_3 with its crystal as plate-like structure. The surface morphology has been modified by the inclusion of Pt nanoparticles in the Bi_2Te_3 , as shown in **Figure 4(b)**. The crystal grain size of $\text{Pt-Bi}_2\text{Te}_3$ composite is smaller than that of pure Bi_2Te_3 , as can be seen in **Figure 4(a)** and **(b)**. Thus, the electrodeposited film with Pt nanoparticles tends to form lower porosity and denser surface structure in comparison to pure Bi_2Te_3 . A high-resolution transmission electron microscopy image of $\text{Pt-Bi}_2\text{Te}_3$ composite is shown in **Figure 4(c)**, where black areas represent the Pt nanoparticles.

Table 2 shows the average grain size calculated by identifying FWHM and Integral Breadth β . As can be seen, the crystal's grain size becomes smaller at higher Pt nanoparticle content. The smallest grain size of 7.9 nm is found at the 1.9 wt% of Pt nanoparticles in the composite, which is four times smaller compared with that of pure Bi_2Te_3 .

The summary of characteristic of the synthesized films is shown in **Table 3**. Experimental results indicate that once the grain size decreases, the carrier

Electrodeposited films	Deposited Pt (wt%)	Integral Breadth, β at $2\theta = 27.7^\circ$, (rad)	Average grain size (nm)
Bi_2Te_3	0.0	0.6×10^{-2}	32.2 ± 4.3
$\text{Pt/Bi}_2\text{Te}_3$ -I	1.0	1.6×10^{-2}	13.9 ± 3.4
$\text{Pt/Bi}_2\text{Te}_3$ -II	1.5	2.2×10^{-2}	10.9 ± 1.3
$\text{Pt/Bi}_2\text{Te}_3$ -III	1.9	3.8×10^{-2}	7.9 ± 0.1

Table 2. Average grain size on Bi_2Te_3 and $\text{Pt-Bi}_2\text{Te}_3$ nanocomposite films at $2\theta = 27.7^\circ$.

Electrodeposited films	Average grain size (nm)	Electrical conductivity (S/cm)	Seebeck coefficient ($\mu\text{V/K}$)	Carrier concentration, n (cm^{-3}) $\times 10^{17}$
Bi_2Te_3	36.5	618.7	-115.2	6.21
Pt (1.0 wt.%)/ Bi_2Te_3	17.3	704.3	-152.1	2.40
Pt (1.5 wt.%)/ Bi_2Te_3	12.1	643.7	-166.6	2.02
Pt (1.9 wt.%)/ Bi_2Te_3	7.80	527.8	-184.1	1.93

Table 3.
 Summary characteristics of the synthesized films.

concentration becomes lower. The lowest carrier concentration is observed for 1.9 wt% Pt- Bi_2Te_3 composite in comparison with others, including Bi_2Te_3 , 1.5 wt% Pt- Bi_2Te_3 , and 1.0 wt% Pt- Bi_2Te_3 . As mentioned in Section 2, the Seebeck coefficient and electrical conductivity are trade-off, and they strongly depend on the carrier concentration. Lower carrier concentration results in a higher Seebeck coefficient but causes the smaller electrical conductivity, which agrees with the observation in this work, as given in **Table 3**.

Figure 5 shows the measurement result of the thermal conductivity of the electrodeposited film. The thermal conductivity decreases as the Pt nanoparticle concentration increases. The main reason is due to a reduction of the phonon mean free path caused by phonon grain boundary scattering [37]. The scattering mechanism of mid- to long-wavelength of phonons in the Pt- Bi_2Te_3 nanocomposite can be imagined via **Figure 5(b)**. Short-wavelength phonons are scattered by imperfections such as atomic defects and stacking defects while the Pt nanoparticles and grain boundaries are effective at scattering the mid- to long-wavelength phonon. A close adjacent between the Pt nanoparticles also contributed to the phonon scattering effect by reducing the phonon mean free path. Based on measurement results, including Seebeck coefficient, electrical conductivity, and thermal conductivity, the maximum ZT for Pt- Bi_2Te_3 nanocomposite is found at 0.61, which is 300% higher than that of the electrodeposited pure Bi_2Te_3 . The details of evaluation setup, measurement results, and other discussions can be found in [24].

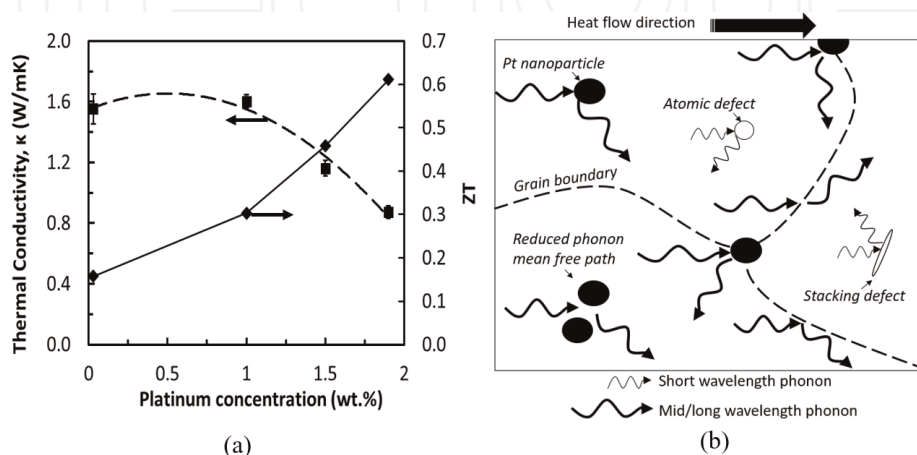


Figure 5.
 Thermal conductivity and ZT as a function of Pt nanoparticle concentration. (b) Illustration of phonon scattering mechanisms in the Pt- Bi_2Te_3 nanocomposite.

In summary, Pt-Bi₂Te₃ nanocomposite has been synthesized successfully by the electrochemical deposition technique. It is found that as higher Pt nanoparticles are deposited in the nanocomposite film, the grain size becomes smaller and the nanostructure experienced significant defects. The change of grain size could be a help to adjust the trade-off between Seebeck coefficient and electrical conductivity, which results in the highest power factor. In addition, the defects caused by Pt nanoparticle benefit the phonon scattering enhancement, thus lowering the thermal conductivity. Consequently, the ZT can be improved.

3.4 Nickel-doped thermoelectric material

Although the thick-film thermoelectric materials have been investigated successfully, as described in Section 3.2, further investigations are still required to enhance their thermoelectric characteristics. Moreover, in order to open an opportunity for mass production, highly scalable synthesis electrodeposition on a large wafer size for thermoelectric materials should be conducted. In this section, a novel process technology for the ultra-thick film as well as high-performance characteristics (high Seebeck coefficient, large electrical conductivity, and low thermal conductivity) is investigated. Both electrodeposited films, including pure Bi₂Te₃ and Ni-doped Bi₂Te₃, reaching in mm-order thickness, have been synthesized, evaluated, and compared. Moreover, a highly scalable electrodeposition process for large wafer size has been performed and proven.

Figure 6(a) and **(b)** show the surface crystal structure of the electrodeposited pure Bi₂Te₃ and Ni-doped Bi₂Te₃, respectively. As can be seen that the crystal grain size of pure

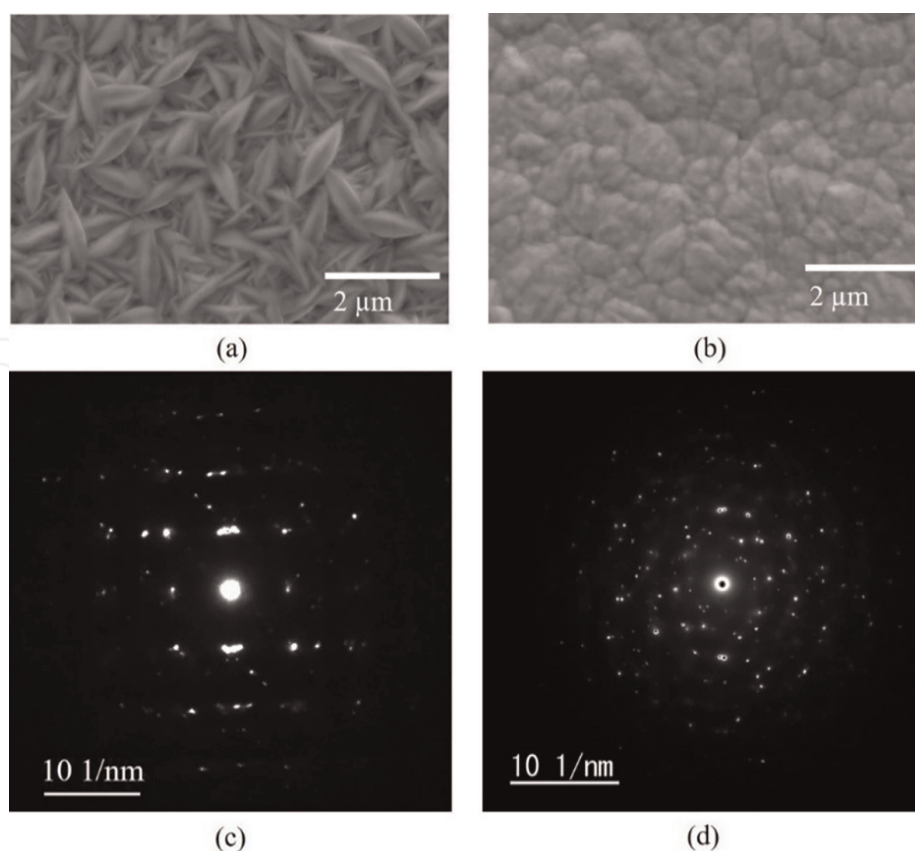


Figure 6. SEM image of pure Bi₂Te₃. (b) SEM image of Ni doped Bi₂Te₃. (c) Selected area electron diffraction pattern of pure Bi₂Te₃. (d) Selected area electron diffraction pattern of pure Ni-doped Bi₂Te₃.

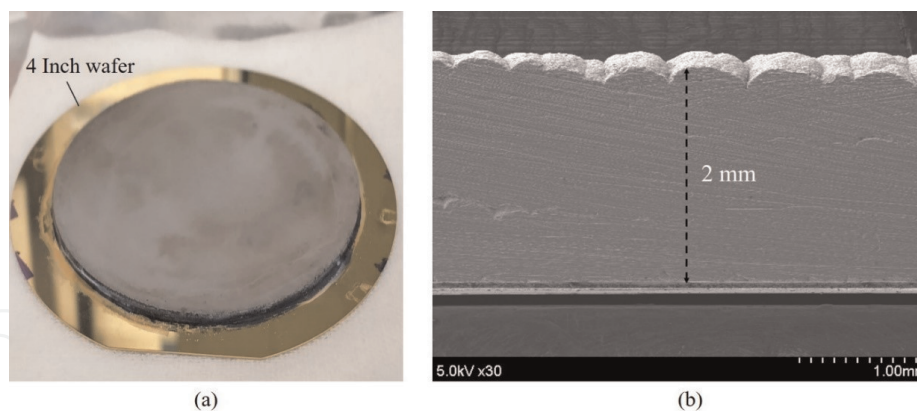


Figure 7. (a) Electrodeposition on 4-inch wafer size. (b) SEM image of the cross-sectional view of the electrodeposited film.

Bi_2Te_3 is much larger than that of Ni-doped Bi_2Te_3 . The selected area electrode diffraction patterns for pure Bi_2Te_3 and Ni-doped Bi_2Te_3 are shown in **Figure 6(c)** and **(d)**, respectively. Diffraction spots in **Figure 6(c)** and **(d)** indicate that both electrodeposited films pose polycrystalline structures. In quantitative comparison, the spots in **Figure 6(d)** are much more than those in **Figure 6(c)**. One possible cause is the grain size effects. Decreasing the grain size results in an increase of the boundary scattering and lattice defects, as discussed in Section 3.3. Thereby, not only the trade-off between Seebeck coefficient and electrical conductivity could be adjusted (changing the carrier concentration), but also the thermal conductivity gets lower due to photon scattering.

Figure 7(a) shows the experimental result of the highly scalable synthesis process, which is performed on a 4-inch wafer size. The deposited film reaches 2 mm thickness with a high uniform surface, as shown in **Figure 7(b)**. The success of the highly scalable electrodeposition could open up the opportunity for mass production to reduce the fabrication cost.

Summary characteristics of the electrodeposited thermoelectric materials can be found in **Table 4**. Experimental results show that 0.7 at% Ni-doped Bi_2Te_3 has the highest Seebeck coefficient as well as largest electrical conductivity compared with others, including pure Bi_2Te_3 , 0.3 at% Ni-doped Bi_2Te_3 , 1.0 at% Ni-doped Bi_2Te_3 , and 1.5 at% Ni-doped Bi_2Te_3 . Although the thermal conductivity of 0.7 at% Ni-doped Bi_2Te_3 is not the smallest one, its thermal conductivity is two times smaller than that of the pure Bi_2Te_3 . The ZT of Ni-doped Bi_2Te_3 is estimated as 0.78, which is five times larger than that of the pure Bi_2Te_3 . The details of evaluation setup, and measurement results, and other discussions can be found in [38, 39].

4. Device fabrication

4.1 Micro-thermoelectric-generator-based on micro/nano fabrication technology

One of the challenges for micro-TEG is the small harvested temperature difference across the module, thus resulting in low output power. In the conventional design of micro-TEG, the heat flows in the vertical direction (thermoelectric elements such as column structure); therefore, ultra-height thermoelectric elements are typically needed. However, to fabricate micro-TEG based on micro/nano technologies, the height of thermoelectric elements is limited to a hundred micrometers due to the

	Seebeck coefficient ($\mu\text{V/K}$)	Electrical conductivity (S/cm)	Power factor ($\mu\text{V/m.K}^2$)	Thermal conductivity (W/m.K)	Figure of merit ZT
Pure Bi_2Te_3	-115 ± 5	525 ± 10	694	1.3 ± 0.1	0.15 ± 0.05
0.3 at% Ni- Bi_2Te_3	-130 ± 5	885 ± 30	1496	0.8 ± 0.05	0.61 ± 0.1
0.7 at% Ni- Bi_2Te_3	-143 ± 4	975 ± 15	2050	0.76 ± 0.09	0.78 ± 0.1
1.0 at% Ni- Bi_2Te_3	-125 ± 5	675 ± 70	1054	0.62 ± 0.04	0.52 ± 0.12
1.5 at% Ni- Bi_2Te_3	-130 ± 10	575 ± 75	972	0.56 ± 0.06	0.5 ± 0.18

Table 4. Summary characteristics of the electrodeposited thermoelectric materials.

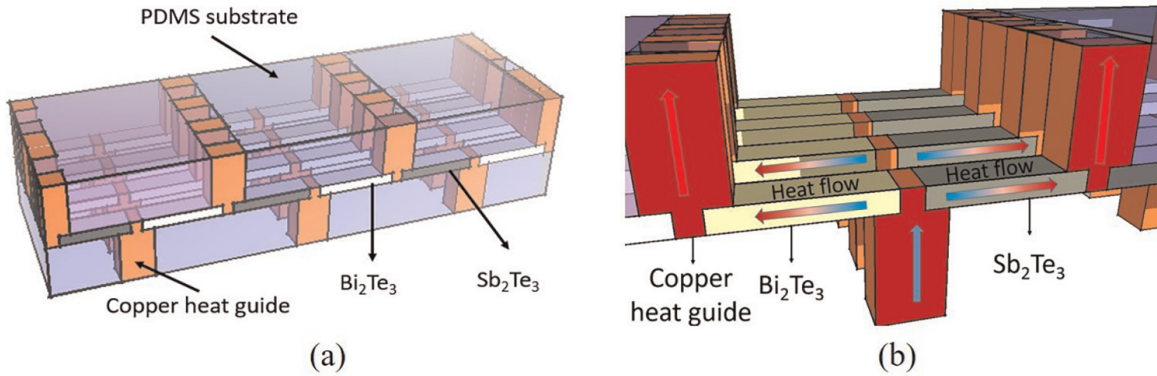


Figure 8. (a) Proposed micro-thermoelectric generator structure. (b) Heat flow in lateral direction.

limitation of the photoresist thickness and a patterning aspect ratio. To overcome this issue, thermoelectric elements are proposed to be laid in a lateral direction instead of a vertical one. The proposed structure for micro-TEG is shown in **Figure 8(a)**, which consists of n- and p-types thermoelectric elements (Bi_2Te_3 and Sb_2Te_3), copper heat guide, and PDMS (polydimethylsiloxane) as a base material. This micro-thermoelectric generator possesses a flexible characteristic that can be utilized in wearable electronic applications. The heat flow direction is shown in **Figure 8(b)**.

Figure 9 shows the fabrication process for micro-TEG, which begins with a silicon wafer. The SiO_2 with 500 nm thickness and Cr-Au layers with 10 nm thickness and 150 nm thickness, respectively, are deposited on the top of the silicon wafer, respectively, by PECVD and sputtering methods (**Figure 9(a)**). The thermoelectric materials are selectively deposited on the Au surface by electrodeposition technique via the patterned photoresist with a thickness of 100 μm (**Figure 9(b)**). Next, Ti-TiN-Au-Cu layer as a barrier contact layer is formed by sputter via a stencil mask, as shown in **Figure 9(c)–(e)**. The copper heat guides are subsequently grown on the barrier contact layer by the electroplating method (**Figure 9(f)**). The front side of micro-TEG is then filled by PDMS (**Figure 9(g)**). To create the heat guide from backside, a deep reactive ion etching (RIE) is conducted (**Figure 9(g)**). A thermal glue with high thermal conductivity is refilled into the molds by a screen printing technique

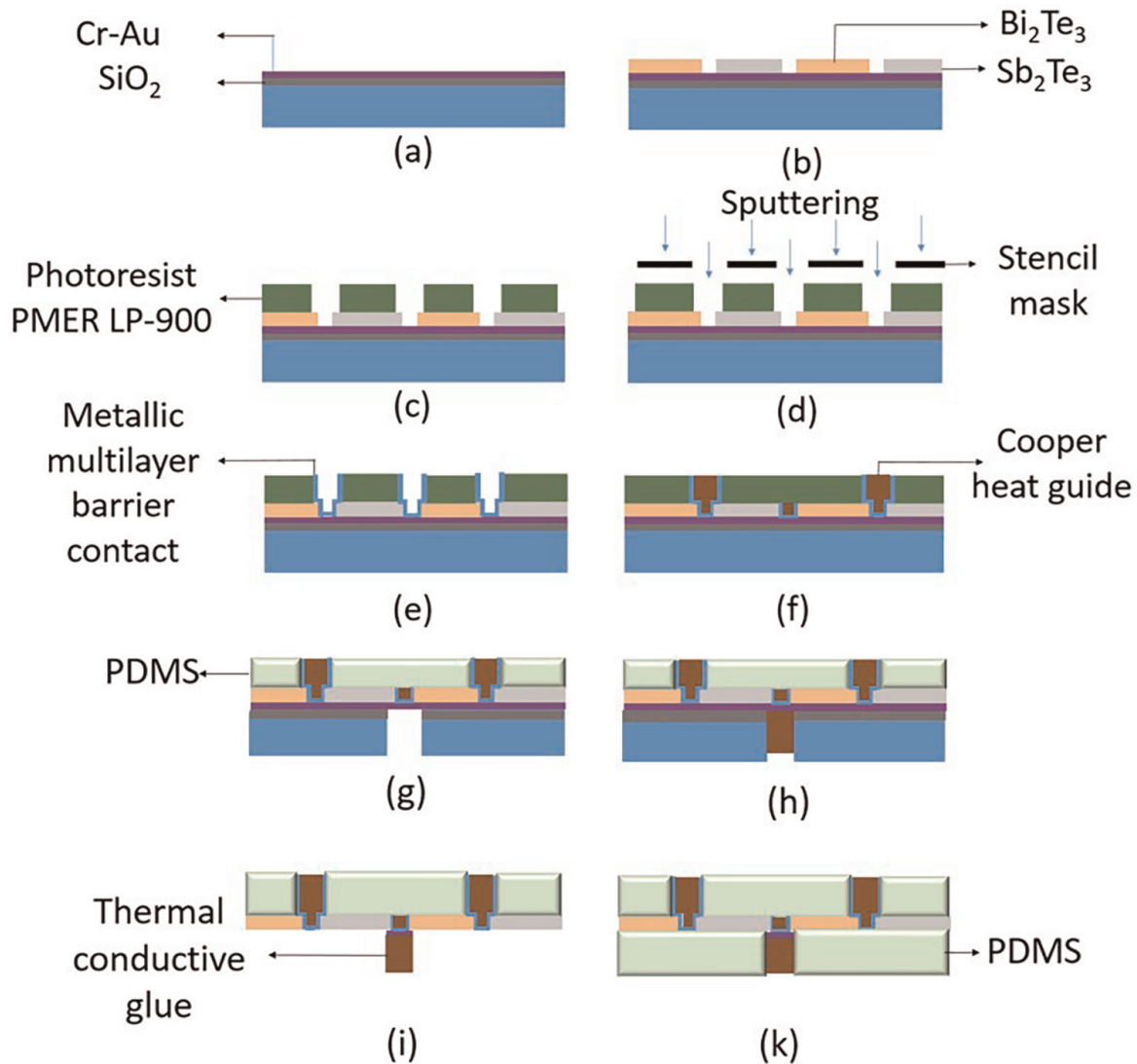


Figure 9. Fabrication process. (a) SiO_2 -Cr-Au deposition. (b) Thermoelectric material synthesis. (c) Photolithography process. (d, e) Multilayers of barrier metal contacts of Ti-TiN-Au-Cu. (f) Copper heat guides. (g) PDMS refilling and Si- SiO_2 removing processes; (h) screen printing process of thermal conductive glue. (i) Backside etching process; (k) PDMS refilling process.

(Figure 9(h)). The remaining silicon layer is etched out by plasma etching, and SiO_2 and Cr-Au layers are removed by the ion beam milling technique (Figure 9(i)). Finally, PDMS is filled into the backside cavities (Figure 9(k)).

Figure 10(a) shows the fabricated micro-TEG based on micro/nano fabrication technologies. The micro-TEG contains 24 pairs of electrodeposited n- and p-type thermoelectric materials integrated on 1 cm^2 . The output power density of the fabricated micro-TEG is displayed in Figure 10(b), which reaches $3\ \mu\text{W}/\text{cm}^2$ under a temperature difference caused by human body (37°C) and ambient environment (15°C) using natural convection. The details of evaluation setup, measurement results, and other discussions can be found in [40].

In summary, a novel design and fabrication process for the micro-TEG have been proposed and investigated. Micro-TEG has been fabricated successfully by micro/nano fabrication technologies. Also, its performance has been evaluated. Although the power density of the fabricated micro-TEG is small, it could be improved by increasing the density of n- and p-types thermoelectric elements. The idea and experimental results in this work may be useful for applications in wearable electronic devices.

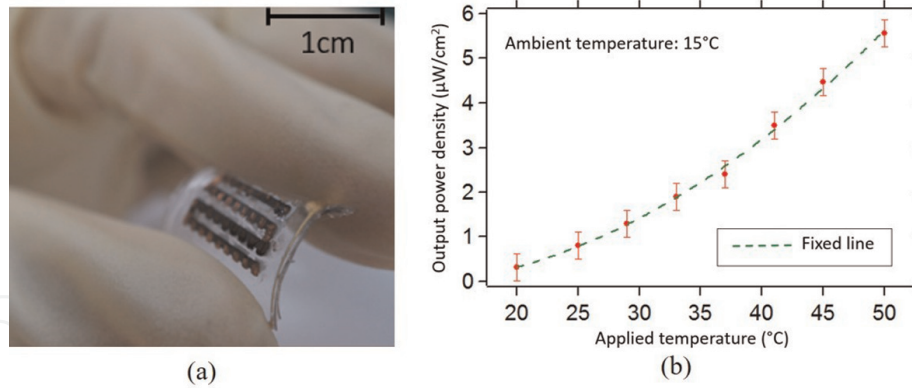


Figure 10. (a) Fabricated micro-TEG. (b) Applied temperature and output power.

4.2 Micro-thermoelectric generator based on assembling technology

To improve the performance of the micro-TEG, enhancing the performance of the thermoelectric materials is a critical point. Another important point is an increase in the number of thermoelectric elements, which can significantly enhance output voltage and output power, as discussed by Eqs. (12) and (13). Thus, the power density can be significantly increased. High-density n- and p-type thermoelectric elements could be formed on a small foot print by utilizing the micro/nano fabrication technologies, as discussed in Section 4.1 and in Refs. [41, 42]. However, some issues need to be addressed, as follows. Complex processes, including photolithography, etching, deposition, and lift-off processes, are needed to construct the air bridge between thermoelectric elements. Therefore, the fabrication time is long, and the cost is high. Moreover, the bonding strength between thermoelectric elements and substrate is weak; thereby, the internal resistance of the fabricated micro-TEG is high, caused by the large contact resistance. Such issues make the performance of the micro-TEG low, which is against it for realistic applications. In this section, a novel method to produce the micro-TEG based on ultra-thick and dense electrodeposited thermoelectric material (presented in Section 3.4) and assembly technique is proposed and investigated.

To fabricate a high-density micro-TEG, small thermoelectric elements are needed, which are prepared as follows. The 4-inch electrodeposited wafer (**Figure 11(a)**) is diced into many small elements (**Figure 11(b)**). It is noted that before cutting, Ni-Au

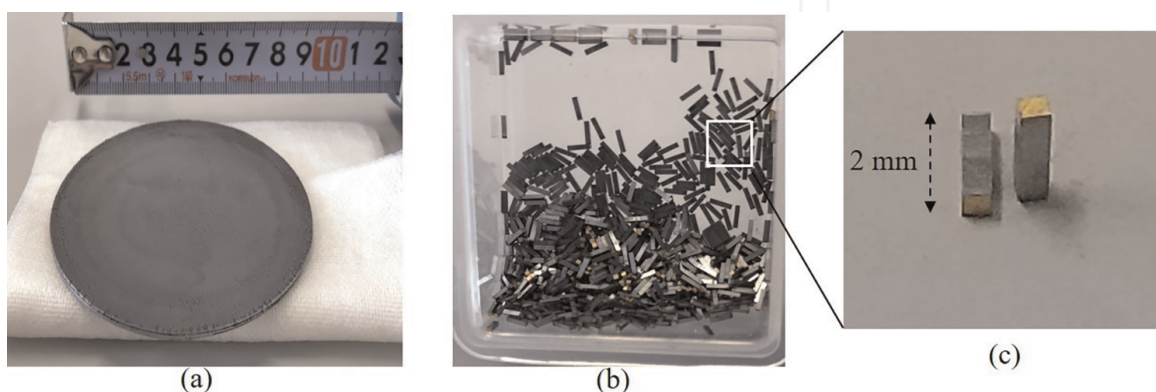


Figure 11. (a) Four-inch electrodeposited thermoelectric material wafer. (b) Thermoelectric elements with dimensions of $0.4 \text{ mm} \times 0.4 \text{ mm} \times 2 \text{ mm}$. (c) Close-up image of thermoelectric elements.

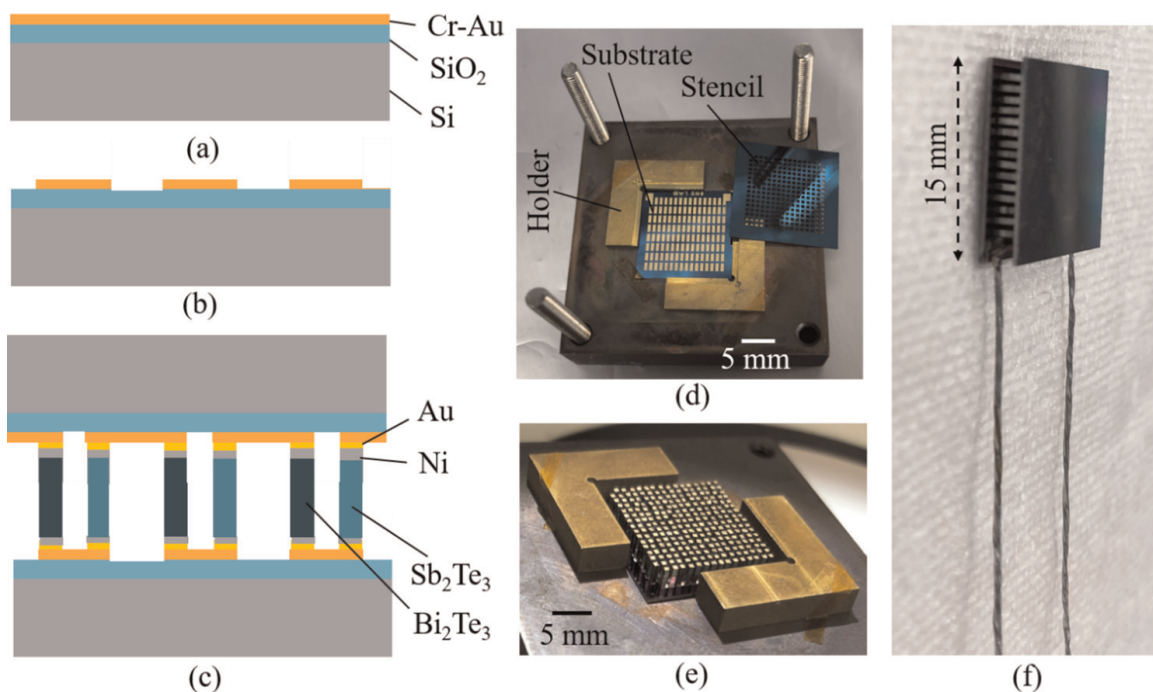


Figure 12. Fabrication process and fabricated micro-TEG. (a) Silicon substrate with SiO_2 and Cr-Au layers on top. (b) Cr-Au patterning. (c) TEG schematic. (d) Device fabrication setup including holders, substrate, and stencil wafer. (e) After the first alignment and bonding. (f) Completely fabricated device.

layers as barrier contact layers are formed on both sides of the wafer by electroplating method [43, 44] to decrease the ohmic contact resistance between thermoelectric elements and substrate. **Figure 11(c)** shows the magnified image of the diced thermoelectric elements with dimensions of $0.4 \text{ mm} \times 0.4 \text{ mm} \times 2 \text{ mm}$.

The fabrication process for the micro-TEG based on the assembly technique is shown in **Figure 12(a)–(c)**. The SiO_2 layer as an insulator layer is formed on a silicon wafer by PECVD, and Cr-Au layers are deposited on the SiO_2 layer by the sputtering method, as given in **Figure 12(a)**. Cr-Au layers are patterned to form the bottom interconnection by a wet etching method [45, 46], as shown in **Figure 12(b)**. Next, thermoelectric elements are aligned and bonded on the substrate by conductive glue. Finally, a top wafer cover is aligned and bonded on top of the thermoelectric elements (**Figure 12(c)**). Because the thermoelectric elements are pretty small, the process for vertical alignment becomes difficult. To overcome this issue, a stencil silicon wafer with patterned through holes is proposed, and a simple metal holder tool is employed to fix and align the stencil wafer and substrate, as shown in **Figure 12(d)**. Thermoelectric elements are inserted into holes of the stencil wafer. **Figure 12(e)** shows the experimental image after the thermoelectric elements are bonded on the substrate. The completely fabricated micro-TEG is shown in **Figure 12(f)**. In total, 127 pairs, including n- and p-type thermoelectric elements, are formed successfully on a small footprint of 15 mm^2 . Thus, although a simple assembly technique is employed, the integration density of thermoelectric elements could be comparable to the micro-fabrication of the micro-TEG.

The fabricated micro-TEG shows a high output power of 33.9 mW and a large power density of 15.1 mW/cm^2 under a temperature difference across the micro-TEG of $75 \text{ }^\circ\text{C}$, which is much higher performance than those of other published works [42, 47–51]. More comparisons to other works are shown in **Table 5**. The details of evaluation setup, measurement results, and other discussions can be found in [52].

Pairs	Height (mm)	Temperature difference ΔT (°C)	Open circuit (V)	Internal resistance (Ω)	Power (mW)	Power density (mW/cm ²)	References
24	0.2	24	0.05	200	—	0.004	[47]
6	0.0015	6	0.036	25	0.0023	—	[48]
71	0.0135	39	0.2	134	2.4	2.4	[49]
127	0.01	52.5	0.3	13	3	9.2	[50]
200	0.02	88	0.5	45.2	—	1.04	[42]
220	2	40	2.1	—	7	1.75	[51]
127	2	75	2.2	35	33.9	15.1	This work [52]

Table 5.
Comparison of TEG performance.

In summary, the high integration density of the micro-TEG has been demonstrated by utilizing a simple assembly technique. Micro-TEG consisting of 127 pairs is successfully fabricated on 15 mm². The fabricated micro-TEG possesses a high performance, which may satisfy the demand for being a reliable power source for electronic devices.

5. Application demonstration

Although a high output voltage and output power could be achieved by the fabricated micro-TEG, a high thermal source is needed. In turn to low-thermal sources, its output power is in small value, which cannot be used as a power source for electronic devices. To overcome this issue, a DC-DC converter is required, which amplifies the output voltage of the micro-TEG from an mV range to V range of the output of the DC-DC converter. Thus, this makes micro-TEG possible for powering electronic devices with low-power consumption. In this section, the micro-TEG for powering calculator and twist watch is demonstrated. A DC-DC converter is utilized to boost the output voltage of the micro-TEG up to sufficient levels to store in an energy-storable unit, which is subsequently supplied to electronic devices. The energy storable unit can be a capacitor, a supercapacitor, or a rechargeable battery. We have developed successfully micro-supercapacitors-based graphene nanowalls with PANI in liquid state [53] and solid state [54] and with MnO₂ [55]. Although these micro-supercapacitors show a high charge and discharge processes, their storable energy is lower than that of commercial rechargeable battery. In this section, a rechargeable battery from Enercera [56] is employed for the application demonstration. Two applications utilizing the micro-TEG are conducted, as follows.

5.1 Micro-TEG for powering portable electronic devices

Figure 13(a) illustrates the experimental setup for the micro-TEG as a power source for the calculator. It consists of Peltier (as a heat source), copper blocks, temperature sensors, the DC-DC converter, a rechargeable battery, and a calculator.

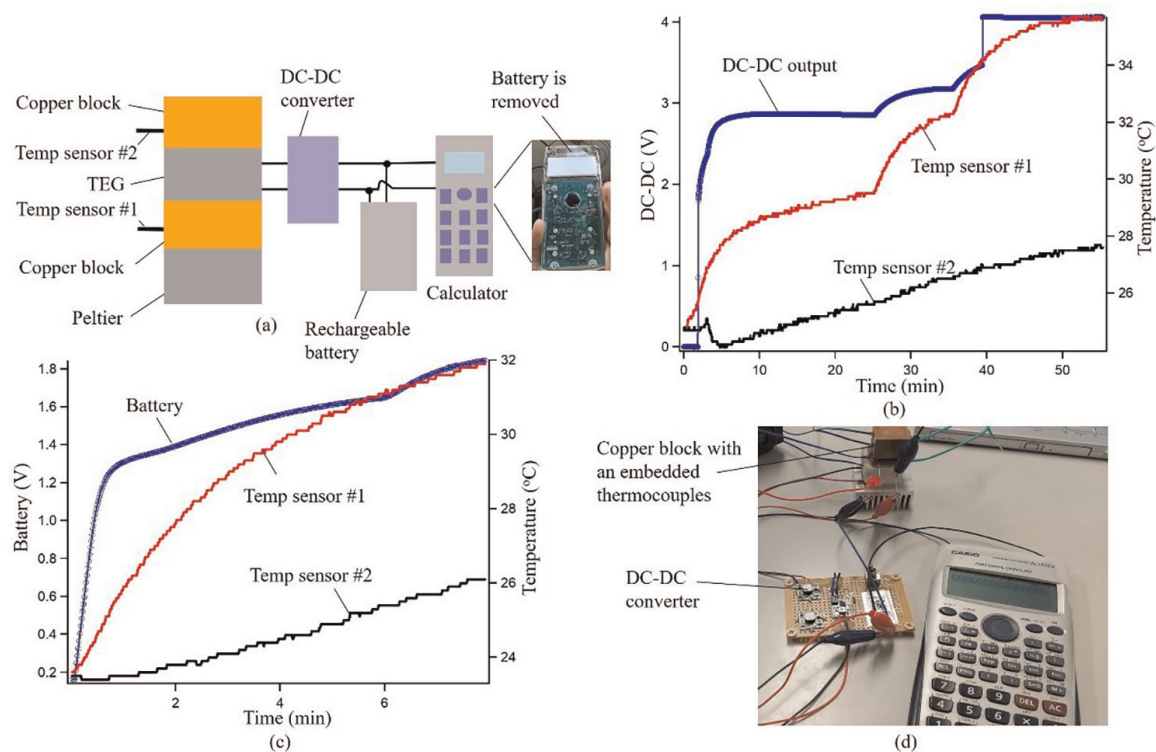


Figure 13. (a) Experimental setup for powering portable electronic device. (b) DC-DC output as a function of temperature difference. (c) Battery charged up by the micro-TEG. (d) Micro-TEG as a power source for calculator.

The harvester energy is accumulated and stored in the rechargeable battery via the DC-DC converter and then supplied to electronic devices. **Figure 13(b)** shows the output of DC-DC converter over the temperature difference across the micro-TEG. The experimental results indicated that output of DC-DC converter reaches 2.8 V at $\Delta T = 2^\circ\text{C}$ and 4 V at $T = 8^\circ\text{C}$. **Figure 13(c)** shows the rechargeable battery characteristic, which increases from 0 V to 1.8 V, taking approximately 8 minutes. **Figure 13(d)** shows the demonstration of using micro-TEG as an electrical power source for the calculator. The calculator can be powered on and used once the rechargeable battery gets over 1.5 V.

5.2 Micro-TEG for powering wearable electronic devices

Figure 14(a) illustrates the experimental setup for powering a twist watch. One side of the micro-TEG is in contact with human skin while another side is attached to the backside of the twist watch. α -Gel is pasted on both sides of the micro-TEG to enhance heat transfer between interfaces. The DC-DC converter and rechargeable battery are employed, which are similar to those mentioned in Section 5.1. The DC-DC converter, rechargeable battery, and micro-TEG are arranged on the twist watch, as shown in **Figure 14(b)**. **Figure 14(c)** shows the output of the micro-TEG and battery charge when twist watch is worn. It takes approximately 5 minutes for the rechargeable battery to reach 1.2 V. With this energy, the twist watch is powered on and runs.

Demonstrated results in this section indicate a high potential using the micro-TEG for powering not only portable electronic devices but also wearable electronic devices. Further integrated functions, including sensing (humidity, temperature, gases, etc.), displaying (screen display), and transmitting (radio frequency, Bluetooth, etc.)

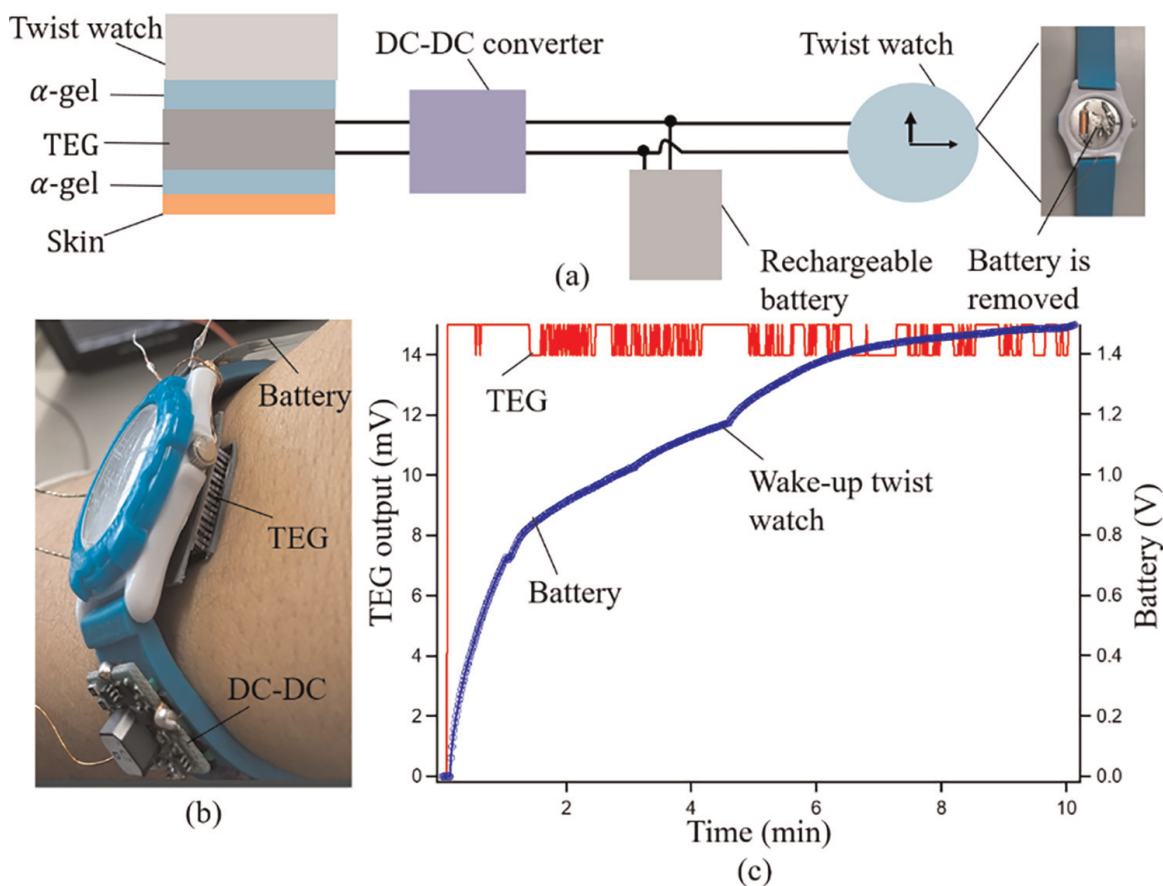


Figure 14. (a) Experimental setup for powering wearable electronic device. (b) The photo of the self-powered twist watch. (c) TEG output and battery charge-up.

functions, should be investigated to produce a smart system for using in wireless IoT sensing systems.

6. Conclusions

In this work, not only basic knowledge about thermoelectric generators but also experiences on material synthesis, device fabrication, and application demonstration are reported. By investigating electrochemical deposition, high-performance thermoelectric materials have been achieved. Three kinds of high-performance thermoelectric materials, including thick bulk-like thermoelectric material, Pt nanoparticles embedded in a thermoelectric material, and Ni-doped thermoelectric material, are reported and discussed. Besides the material synthesis, novel fabrication methods can also help increase the output power and the power density of the micro-TEG significantly. Two fabrication processes, micro/nano fabrication technology and assembly technology, are investigated to produce high-performance micro-TEG. Moreover, the fabricated micro-TEG is successfully demonstrated for powering portable and wearable electronic devices. The contents of this paper are based on our experimental research. It is our hope that this review may be a useful reference for those working in the field of thermal-to-electric energy conversion, especially on the micro-TEG.

Acknowledgements

Part of this work was performed in the Micro/Nanomachining Research Education Center (MNC) of Tohoku University. This work was supported by Cabinet Office, Government of Japan, Cross-ministerial Strategic Innovation Promotion Program (SIP), (funding agency: The New Energy and Industrial Technology Development Organization, NEDO) and also supported in part by JSPS KAKENHI for Young Scientists (Grant number: 20K15147).

Author details

Nguyen Van Toan^{1*}, Truong Thi Kim Tuoi², Nguyen Huu Trung³,
Khairul Fadzli Samat⁴, Nguyen Van Hieu⁵ and Takahito Ono^{1,2*}

1 Micro System Integration Center, Tohoku University, Sendai, Japan

2 Graduate School of Engineering, Tohoku University, Sendai, Japan


3 National Institute of Industrial Science and Technology, Nagoya, Japan

4 Fakulti Kejuruteraan Pembuatan, Universiti Teknikal Malaysia Melak, Melaka, Malaysia

5 Department of Physics and Electronic Engineering, University of Science, VNU-HCM, Vietnam

*Address all correspondence to: nguyen.van.toan.c6@tohoku.ac.jp;
takahito.ono.d4@tohoku.ac.jp

IntechOpen

© 2022 The Author(s). Licensee IntechOpen. This chapter is distributed under the terms of the Creative Commons Attribution License (<http://creativecommons.org/licenses/by/3.0>), which permits unrestricted use, distribution, and reproduction in any medium, provided the original work is properly cited. 

References

- [1] Chang SY, Cheng P, Li G, Yang Y. Transparent polymer photovoltaics for solar energy harvesting and beyond. *Joule*. 2018;**2**:1039-1054
- [2] Tran LG, Cha HK, Park WT. RF power harvesting: A review on designing methodologies and applications. *Micro and Nano Systems Letters*. 2017;**5**:14
- [3] Toan NV, Hasana MMIM, Udagawa D, Inomata N, Toda M, Said SM, et al. Thermoelectric generator battery using 10 nm diameter of Al₂O₃ nanochannels for low-grade waste heat energy harvesting. *Energy Conversion and Management*. 2019;**199**:111979
- [4] Tuoi TTK, Toan NV, Ono T. Theoretical and experimental investigation of a thermoelectric generator (TEG) integrated with a phase change material (PCM) for harvesting energy from ambient temperature changes. *Energy Reports*. 2020;**6**: 2022-2029
- [5] Haras M, Skotnicki T. Thermoelectricity for IoT – A review. *Nano Energy*. 2018;**54**:461-476
- [6] Tuoi TTK, Toan NV, Ono T. Heat storage thermoelectric generator as an electrical power source for wireless IoT sensing systems. *International Journal of Energy Research*. 2021;**45**:15557-15568
- [7] Zhou Y, Liu Y, Zhou X, Gao Y, Gao C, Wang L. High performance p-type organic thermoelectric materials based on metalloporphyrin/single-walled carbon nanotube composite films. *Journal of Power Sources*. 2019;**423**: 152-158
- [8] Xu S, Liu C, Xia Z, Zhong W, Luo Y, Ou H, et al. Cooperative effect of carbon black and dimethyl sulfoxide on PEDOT: PSS hole transport layer for inverted planar perovskite solar cells. *Solar Energy*. 2017;**158**:125-132
- [9] Toshima N, Jiravanichanun N, Marutani H. Organic thermoelectric materials composed of conducting polymers and metal nanoparticles. *Journal of Electronic Materials*. 2012;**41**: 1735-1742
- [10] Li Y, Toan NV, Wang Z, Samat KF, Ono T. Thermoelectrical properties of silicon substrates with nanopores synthesized by metal-assisted chemical etching. *Nanotechnology*. 2020;**31**: 455805
- [11] Sabran NH, Fadzallah IA, Ono T, Said SM, Sabri MFM. Preparation and characterization of electrochemical deposition cobalt triantimonide (CoSb₃) thick film: Effect of polyvinyl alcohol (PVA) as an additive. *Journal of Electrochemical Materials*. 2019;**48**: 5003-5011
- [12] Tuoi TTK, Toan NV, Ono T. Heat storage thermoelectric generator for wireless IoT sensing systems. In: *The 21st International Conference on Solid-State Sensors, Actuators and Microsystems (Transducers)*. Orlando, FL, USA: IEEE; 2021. pp. 924-927. DOI: 10.1109/Transducers50396.2021.9495686
- [13] Zhang Y, Xing C, Zhang T, Li M, Pacios M, Yu X, et al. Tin selenide molecular precursor for the solution processing of thermoelectric materials and devices. *ACS Applied Materials & Interfaces*. 2020;**12**: 27104-27111
- [14] Ono T, Nguyen TH, Samat KF, Li J, Toan NV. Nanoengineered thermoelectric energy devices for IoT

sensing applications. ECS Transactions. 2019;**92**:163-168

[15] Dheepa J, Sathyamoorthy R, Velumani S, Subbarayan A, Natarajan K, Sebastian PJ. Electrical resistivity of thermally evaporated bismuth telluride thin films. *Solar Energy Materials and Solar Cells*. 2004;**81**:305-312

[16] Bendt G, Gassa S, Rieger F, Jooss C, Schulz S. Low-temperature MOCVD deposition of Bi₂Te₃ thin films using Et₂BiTeEt as single source precursor. *Journal of Crystal Growth*. 2018;**490**: 77-83

[17] Carter MJ, Desouky AE, Andre MA, Bardet P, Leblance S. Pulsed laser melting of bismuth telluride thermoelectric materials. *Journal of Manufacturing Processes*. 2019;**43**:35-46

[18] Rosi FD. Thermoelectricity and thermoelectric power generator. *Solid State Electronics*. 1968;**11**:833-868

[19] Heremans JP, Jovovicm V, Toberer ES, Saramat A, Kurosaki K, Charoenphakdee A, et al. Enhancement of thermoelectric of the electronic density of states. *Science*. 2008;**321**: 1457-1461

[20] Pei Y, Shi X, Lalonde A, Wang H, Chen L, Snyder GJ. Convergence of electronic bands for high performance bulk thermoelectrics. *Nature*. 2011;**473**: 66-69

[21] Rosi FD. Thermoelectricity and thermoelectric power generation. *Solid-State Electronics*. 1968;**11**:833-848

[22] Chasmar RP, Stratton R. The thermoelectric figure of merit and its relation to thermoelectric generators. *Journal of Electronic and Control*. 1959;**7**: 52-57

[23] Hodes M. Optimal pellet geometries for thermoelectric power generation. *IEEE Transactions on Components and Packaging*. 2010;**33**:307-318

[24] Samat KF, Trung NH, Ono T. Enhancement in thermoelectric performance of electrochemically deposited platinum-bismuth telluride nanocomposite. *Electrochimica Acta*. 2019;**312**:62-71

[25] Li Y, Toan NV, Wang Z, Samat KF, Ono T. Formation and evaluation of silicon substrate with highly-doped porous Si layers formed by metal-assisted chemical etching. *Nanoscale Research Letters*. 2021;**16**:64

[26] Samat KF, Li Y, Toan NV, Ono T. Carbon black nanoparticles inclusion in bismuth telluride film for micro thermoelectric generator application. In: *The 33rd IEEE International Conference on Micro Electro Mechanical Systems*. Vancouver, BC, Canada: IEEE; 2020. pp. 562-565

[27] Kim C, Yang Y, Baek JY, Lopez DH, Kim DH, Kim H. Concurrent defects of intrinsic tellurium and extrinsic silver in an n-type Bi₂Te_{2.88}Se_{0.15} thermoelectric materials. *Nano Energy*. 2019;**60**:26-35

[28] Ming T, Yang W, Huang X, Wu Y, Li X, Liu J. Analytical and numerical investigation on a new compact thermoelectric generator. *Energy Conversion and Management*. 2017;**132**: 261-271

[29] Macia E. *Thermoelectric Materials: Advances and Applications*. New York: Stanford Publishing; 2015. p. 364

[30] Kanani N. Chapter 5 – Electrodeposition considered at the atomistic level. In: *Electroplating*. Elsevier; 2004. pp. 141-177. DOI: 10.1016/B978-185617451-0/50005-1

- [31] Bicer M, Sisman I. Electrodeposition and growth mechanism of SnSe thin films. *Applied Surface Science*. 2011;**257**: 2944-2949
- [32] Ma Y. Thermoelectric characteristics of electrochemically deposited Bi₂Te₃ and Sb₂Te₃ thin films of relevance to multilayer preparation. *Journal of the Electrochemical Society*. 2012;**159**:50
- [33] Trung NH, Sakamoto K, Toan NV, Ono T. Synthesis and evaluation of thick films of electrochemically deposited Bi₂Te₃ and Sb₂Te₃ thermoelectric materials. *Materials*. 2017;**10**:154
- [34] Lee E, Ko J, Kim JY, Seo WS, Choi SM, Lee KH, et al. Enhanced thermoelectric properties of Au nanodot-included Bi₂Te₃ nanotube composites. *Journal of Materials Chemistry C*. 2016;**4**(6):1313-1319
- [35] Zhang Q, Ai X, Wang L, Chang Y, Luo W, Jiang W, et al. Improved thermoelectric performance of silver nanoparticles-dispersed Bi₂Te₃ composites deriving from hierarchical two-phased heterostructure. *Advanced Functional Materials*. 2015;**25**(6): 966-976
- [36] Sun T, Samani MK, Khosravian N, Ang KM, Yan Q, Tay BK, et al. Enhanced thermoelectric properties of n-type Bi₂Te_{2.7}Se_{0.3} thin films through the introduction of Pt nanoinclusions by pulsed laser deposition. *Nano Energy*. 2014;**8**:223-230
- [37] Touzelbaev MN, Zhou P, Venkatasubramanian R, Goodson KE. Thermal characterization of Bi₂Te₃/Sb₂Te₃ superlattices. *Journal of Applied Physics*. 2001;**90**:763
- [38] Toan NV, Tuoi TTK, Ono T. Thermoelectric generators for heat harvesting: From material synthesis to device fabrication. *Energy Conversion and Management*. 2020;**225**:113442
- [39] Toan NV, Tuoi TTK, Samat KF, Sui H, Inomata N, Toda M, et al. High performance micro-thermoelectric generator based on metal doped electrochemical deposition. In: *The 33rd IEEE International Conference on Micro Electro Mechanical Systems*. Vancouver, BC, Canada: IEEE; 2020. pp. 570-573
- [40] Trung NH, Toan NV, Ono T. Electrochemical deposition based flexible thermal electric power generator with Y-type structure. *Applied Energy*. 2018;**210**:467-476
- [41] Synder GJ, Jim JR, Huang CK, Fleurial JP. Thermoelectric microdevice fabricated by a MEMS-like electrochemical process. *Nature Materials*. 2003;**2**:528-531
- [42] Yu Y, Zhu W, Wang Y, Zhu P, Peng K, Deng Y. Towards high integration and power density: Zigzag-type thin-film thermoelectric generator assisted by rapid pulse laser patterning technique. *Applied Energy*. 2020;**285**: 115404
- [43] Toan NV, Sangu S, Ono T. Fabrication of deep SiO₂ and Tempax glass pillar structures by reactive ion etching for optical modulator. *Journal of Microelectromechanical Systems*. 2016; **25**:668-674
- [44] Toan NV, Sangu S, Ono T. High aspect ratio SiO₂ pillar structures capable of the integration of an image sensor for application of optical modulator. *IEEE Transactions on Sensors and Micromachines*. 2016;**136**:41-42
- [45] Toan NV, Toda M, Ono T. An investigation on etching techniques for glass micromachining. *Micromachining*. 2016;**7**:51

- [46] Toan NV, Ono T. Progress in performance enhancement methods for capacitive silicon resonators. *Japanese Journal of Applied Physics*. 2017;**56**: 110101
- [47] Trung NH, Toan NV, Ono T. Fabrication of π -type flexible thermoelectric generators using an electrochemical deposition method for thermal energy harvesting applications at room temperature. *Journal of Micromechanics and Microengineering*. 2017;**27**:125006
- [48] Shen H, Lee H, Han S. Optimization and fabrication of a planar thermoelectric generator for a high-performance solar thermoelectric generator. *Current Applied Physics*. 2021;**22**:6-13
- [49] Roth R, Rostek R, Cobry K, Kohler C, Groh M, Woias P. Design and characterization of micro thermoelectric cross-plane generators with electroplated Bi_2Te_3 , Sb_2Te_3 , and reflow soldering. *Journal of Microelectromechanical Systems*. 2014;**23**: 961-971
- [50] Zhang W, Yang J, Xu D. A high power density micro-thermoelectric generator fabricated by an integrated bottom-up approach. *Journal of Microelectromechanical Systems*. 2016; **25**:744-749
- [51] Lee B, Cho H, Park KT, Kim JS, Park M, Kim H, et al. High-performance compliant thermoelectric generators with magnetically self-assembled soft heat conductors for self-powered wearable electronics. *Nature Communications*. 2020;**11**:5948
- [52] Toan NV, Tuoi TTK, Hieu NV, Ono T. Thermoelectric generator with a high integration density for portable and wearable self-powered electronic devices. *Energy Conversion and Management*. 2021;**245**:114571
- [53] Li J, Toan NV, Wang Z, Ono T. Metal-assisted chemical etching of silicon nanowires for templating 3D graphene growth towards energy storage in microsystems. *Journal of Micromechanics and Microengineering*. 2019;**29**:055077
- [54] Toan NV, Tuoi TTK, Li J, Inomata N, Ono T. Liquid and solid states on-chip micro-supercapacitors using silicon nanowire-graphene nanowall-PANI electrode based on microfabrication technology. *Materials Research Bulletin*. 2020;**131**:110977
- [55] Sui H, Toan NV, Ono T. Vertically-oriented graphene electrodeposited with MnO_2 on native SiO_2/Si for high-performance supercapacitor electrodes. *Journal of Electroanalytical Chemistry*. 2021;**895**:115507
- [56] Available from: <https://www.ngk-insulators.com/en/product/enercera.html> [Accessed: January 12, 2022]